EXPERIMENTAL VALIDATION OF ROBUSTNESS AGAINST FAILURES OF A FAIL-SAFE ELECTRO-MECHANICAL ACTUATOR EMPLOYED FOR THE FLAP MOVABLES OF A HIGH-SPEED HELICOPTER-PLANE

Gianpietro Di Rito, University of Pisa - Dept. of Civil and Industrial Engineering, Pisa, Italy
Romain Kovel, Airbus Helicopters, Marignane, France
Benedetto Luciano, AESIS, San Giuliano Terme, Italy
Federico Salvi, Umbragroup, Foligno, Italy
Marco Nardeschi, Umbragroup, Foligno, Italy

Abstract

The work summarizes the main experimental results carried out for the performance qualification of a fail-safe rotary electro-mechanical actuator employed to control the flap movables of the Airbus RACER helicopter-plane. The RACER flaps, placed on both box-wing and vertical stabilizers, are used to adapt the vehicle attitude, to enhance stability, and to abate noise. Being the actuator requirements driven by disturbance-rejection capabilities, a special attention is dedicated to tests of quasi-static position-tracking and position-hold under high load disturbances, by characterizing the transients related to artificial injection of faults. The worst-case load scenarios are reproduced on a hydraulic test rig, equipped with four servo-actuators, to apply bending moment, axial and radial forces, and torsional hinge moment. Thanks to a closed-loop position control integrating cascade loops on motor currents, motor speed and output rotation with a deformation loop for stiffness enhancement, the position deviation during experiments is minimized when the actuator works without faults. If major faults are injected, the monitoring algorithms succeed in promptly detecting them and the actuator is reverted in fail-safe blocked mode, with failure transients limited by a specifically-designed back-electromotive damper circuitry.

1. INTRODUCTION

Aircraft electrification, being one of the key factors to achieve the Flight Path 2050 goals (Ref. 1), is nowadays one of the most important drivers of the aviation industry innovation. By leveraging more-electric design concepts, future aircrafts could actually benefit from reduced weight, reduced maintenance costs, improved power efficiency and increased eco-compatibility, thanks to lower noise and CO_2 emissions (Refs. 2-4). Electro-mechanical actuation clearly plays a key role for pursuing these objectives. The applicability of Electro-Mechanical Actuators (EMAs) in aerospace is well proven in terms of load and speed performances, but reliability still remains an open issue (Refs. 5-8). Considering the failure rates of mechanical, electrical and electronic components at the current state-of-art, fault-tolerant capabilities must be implemented in EMAs employed for safety-critical functions, in order to be minimize, at aircraft-level, the effects of actuator major faults. One of the most challenging activities during EMA qualification is the demonstration of robustness against failures, with particular reference to failure transient characterization. These analyses can be preliminarily developed by means of high-fidelity dynamic models including faults simulation (Refs. 9-10), but the equipment qualification is achieved only when successful experiments are carried out. This work, substantiating the simulation studies conducted by the authors in Ref. 10, summarizes the experimental activities carried out for the qualification of performances of a fail-safe rotary EMA developed by Umbragroup (Italy) and employed for the control of the flap movables of the RACER helicopter-plane by Airbus Helicopters, with particular focus on the validation of robustness against failures.

2. SYSTEM DESCRIPTION

2.1. EMAs for the RACER flaps

In the RACER helicopter-plane, four flaps are placed on the box-wing and two ones on the vertical stabilizers (Figure *1*). The movables are used to adapt the vehicle attitude, to enhance stability, to optimize the trim configuration, and to abate noise (Refs. 11-12). Depending on the vehicle weight, the airspeed, the altitude, and the rotors speed, the wing flaps are deflected to optimize the lift coefficient of the main rotor, while the flaps on the vertical fins are used to eliminate residual yawing torques generated by the propellers, assuring they contribute to propulsion only during cruise (Ref. 13). The flaps are not used for maneuverability (trajectory control is managed through the cyclic stick, as for conventional helicopters), so that they are classified as secondary flight controls. The flap EMAs are thus designed to be fail-safe systems, so that, after a major fault, the actuator is still capable of maintaining the movable at a fixed deflection (last or neutral position, depending on the fault mode), providing an adequate torsional stiffness to avoid flutter concerns. Each EMA is composed of two parts (Figure 2): an electromechanical rotary actuator (Figure 3) and a control electronic box (Figure 4).

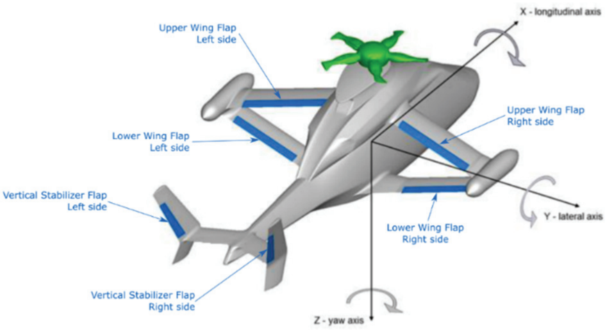

Figure 1: Flap movables of the Airbus RACER helicopter-plane.

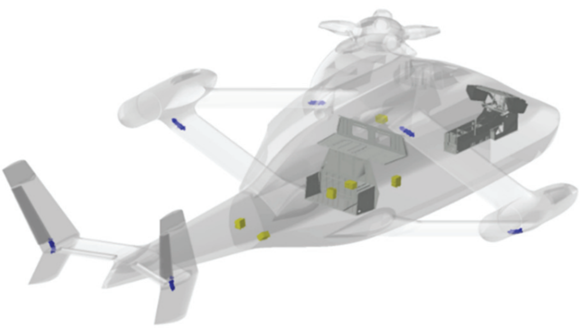

Figure 2: Electro-mechanical actuation system of the flap movables of the Airbus RACER helicopter-plane (control boxes in yellow, actuators in blue).

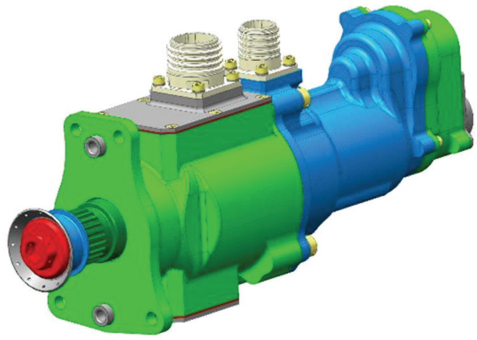

Figure 3: Layout of the electro-mechanical rotary actuator (courtesy from Umbragroup).

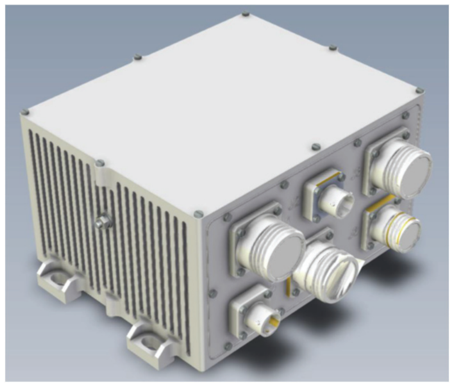

Figure 4: Layout of the electronic control box (courtesy from Umbragroup).

2.2. Mechanical transmission and electric motor

The mechanical transmission of the flap EMAs is based on a high-ratio direct drive design, based on an innovative differential screw mechanisms patented by Umbragroup. The complete elimination of gears permits to reduce complexity, increase stiffness, decrease backlash, enhance reliability, maintain efficient operation across large temperature ranges, and abate noise. With reference to Figure 5, the working principle of the Umbragroup-patented mechanical transmission can be described as follows:

- the rotation of the rotor shaft of the electric motor (a) implies the rotation of the so-called input screw (b), directly connected to it;
- the roto-translating screw (c), internally coupled to the input screw by the pitch P1 and externally coupled to a fixed ball-nut (d) by the pitch P2, translates along the longitudinal axis of the actuator and rotates wrt input screw with a ratio that depends on the ratio of the pitches;
- the translational joint (e) permits the roto-translating screw to freely translate while transmitting its rotation to the output shaft (f);

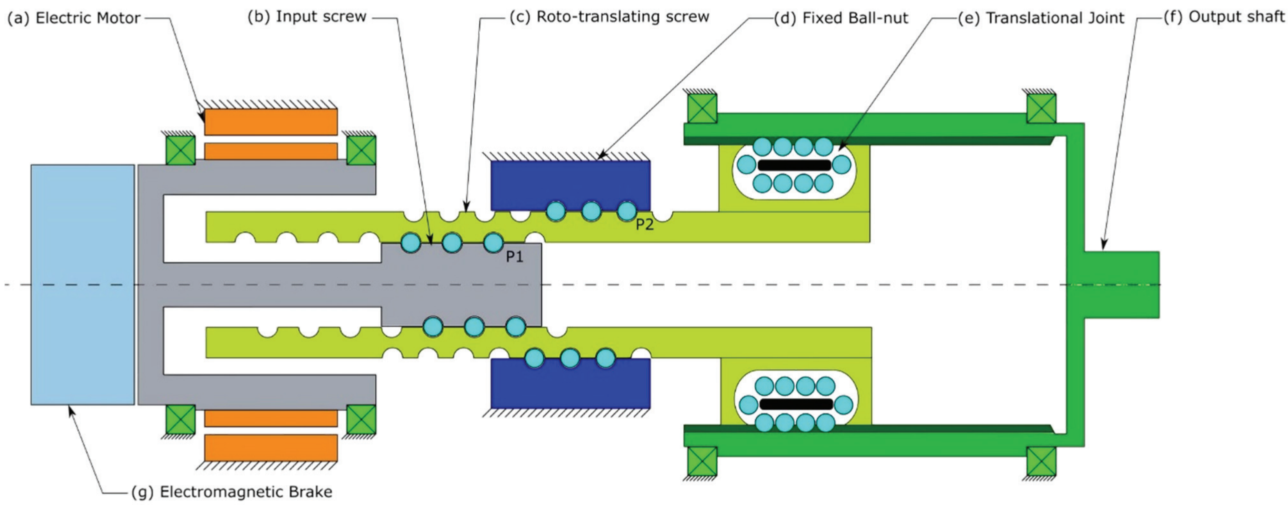

Figure 5: Schematics of the RACER flap EMA mechanical transmission.

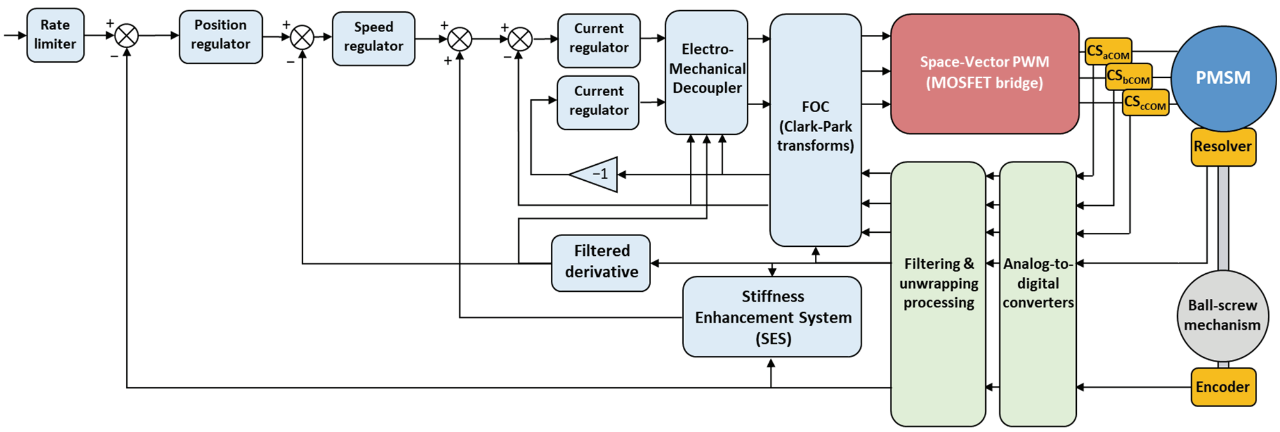

Figure 6: Schematics of the RACER flap EMA closed-loop control.

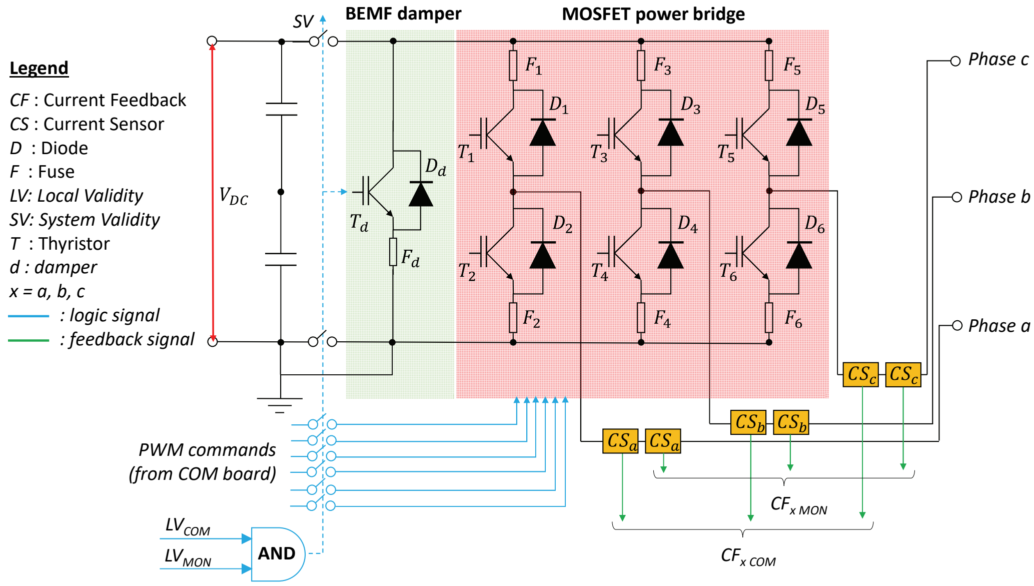

Figure 7: Schematics of the RACER flap EMA power electronics with back-electromotive damper circuitry.

- an electromagnetic power-off brake (g) is integrated with the EMA assembly to lock the output shaft in case of de-energized system (shutdown or motor without power) or in case of detection of a major fault (fail-safe requirement).

Concerning the electric motor, the RACER flap EMA integrates a three-phase permanent magnet synchronous machine with surface-mounted magnets, characterized by high power density (211 kW/kg) and low torque ripple (<1.5% of the maximum motor torque).

2.3. Control and power electronics

The electronic control box of the RACER flap EMA includes three boards: a command board, a monitor board, and a power board, assuring the electrical supply and the power regulation for all EMA components.

The closed-loop control, executed at 10 kHz sampling frequency by the command board, can be described with reference to the block diagram in Figure 6. The architecture integrates three conventional nested loops on motor currents, motor speed, and output position with a deformation loop ("SES" block in Figure 6). The input for the outer position regulator is the rotation command received from the flight control system, processed by a rate-limiting function. The intermediate speed loop receives as input the rotation tracking error, while the quadrature current regulator (FOC technique is applied) receives as input the speed tracking error and an additional current request depending on torsional deformation (conventional null request is provided to the direct current regulator). All regulators implement proportional/integral actions and anti-windup functions with a back-calculation technique. The deformation loop is used to enhance the rejection of load disturbances in the frequency range where the first resonant pulsation of the mechanism is located (depending on working position, from 70 to 90 Hz).

2.4. Monitoring and fail-safe mode engagement

Both control and monitor boards execute, at 10 kHz sampling frequency, monitoring algorithms based on threshold checks with confirmation latency. Each monitored signal is compared to a pre-defined threshold and in case the threshold is exceeded, a fault detection counter is triggered. If the counter exceeds a pre-defined value of confirmation cycles, a Boolean validity flag is initialized and the fail-safe mode engagement is commanded (the EMA must be locked in place by the brake). Considering that a complete brake engagement can be assured only after 50 ms, one of the basic design issues is clearly related to the EMA failure transient. As discussed in Ref. 10, the failure transient of the RACER flap EMA is actually limited by integrating a BEMF damper circuitry in the power electronics. As shown in Figure 7, the circuitry activation is given by the so-called Signal Validity flag (SV), which derives from an "AND" operator applied to the local validity signals generated by the monitoring algorithms executed in the two boards of the EMA (LV_{COM} and LV_{MON}, in Figure 7). If SV is true, the power bridge thyristors are opened, and the damper thyristor is closed, so that the motor phases are shorted to the ground, and an electromagnetic damping torque is transmitted to the output shaft.

The following set of health-monitoring functions are implemented in the RACER flap EMA control boards:

- over-temperature of the motor stator, with 130 °C threshold and 3 ms latency;
- over-current of the motor, with 5 A threshold and 3 ms latency;
- unbalanced three-phase circuitry, with threshold of 350 mA on the sum of phase currents and 4 ms latency;
- torsional deformation consistency, with 2.2° threshold and 13 ms latency;
- motor over-speed (Over-Speed Monitor, OSM), with thresholds of 1°/s on the motor speed and 0.25° on position deviation and 7 ms latency;
- excessive position error, with 0.45° threshold and 4 ms latency.

2.5. Hydraulic multi-axes test rig

A hydraulic test rig has been specifically-designed at Umbragroup premises to reproduce the worst case load scenarios, using four servo-controlled actuators to apply torsional moment, bending moment, axial and radial forces, respectively, Figure 8. Extensive tests have been carried out with high-frequency/large-amplitude harmonic hinge moments, by achieving +/−29.5 Nm at the principal rotor frequency (23.25 Hz). A relevant part of the testing activities has been devoted to the validation of robustness against failures, which has been obtained by artificially injecting disturbances, errors and signal corruptions to reproduce the most critical EMA failures (overspeed, loss of the output position sensor, loss of a current sensor) and characterizing the failure transients in terms of position deviations.

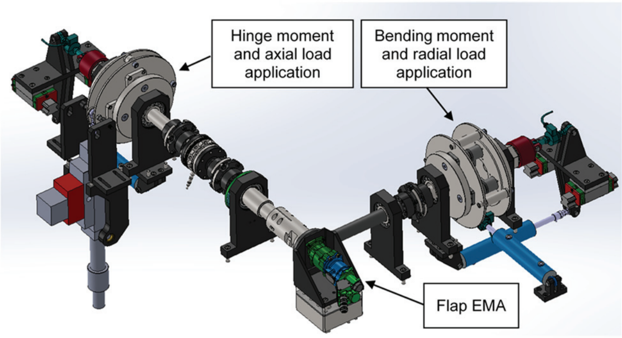

Figure 8: Multi-axes loading test rig used for the RACER flap EMA qualification.

2.6. Test campaign definition

The qualification of the RACER flap EMA has been carried by executing, for three different values of the rigging installation angle (centred and maxima opposite angles wrt flap):

- stall load test, in which the EMA is operated to apply increasing values of torque while the output shaft is locked by the test bench.
- gust load test, in which the EMA is commanded to hold the centred position under different load scenarios, i.e.
  - torsional moment from 225 Nm up to 311 Nm (wing flap requirements)
  - static radial loads up to 2207 N
  - static axial compressive load up to 800 N
  - static bending moment applied on the output flange up to 50 Nm
- disturbance-rejection tests, in which the EMA is commanded to hold a position (centred or at endstrokes) under different load scenarios, i.e.
  - static torsional moment up to 209 Nm (wing flap requirement)
  - harmonic torsional moment up to 30 Hz frequency with amplitudes up to 29.5 Nm (vertical fin flap requirement)
  - static radial loads up to 1260 N
  - static axial compressive load up to 725 N
  - static bending moment applied on the output flange up to 29 Nm
- position-tracking tests, in which the EMA is commanded to move at constant speed under the load scenarios defined above;
- performance robustness against temperature, by integrating a thermal chamber enveloping the EMA and the ECU with the multi-axes loading test rig, to verify (for a subset of test cases) the correct operation at environment temperatures from −33°C to 73°C
- failure transient tests, in which, while the EMA is approaching at constant speed its endstroke under a static hinge moment applied in the direction of motion (worst case), the following major faults are artificially injected:
  - f1. current sensor fault (frozen or full-scale value)
  - f2. ADC fault (all current sensors provide corrupted signals)
  - f3. motor angle sensor fault (frozen value)
  - f4. output angle sensor fault (frozen value)
  - f5. command voltage hardover fault (full-scale value)

3. RESULTS AND DISCUSSION

3.1. Relevant test cases and requirements

An excerpt of the results of the qualification campaign is presented, as summarized in Table 1 (note that the test B.f4 is related to the injection of a frozen value of output angle sensor, as described in section 2.6). Concerning dynamic performance requirements, it is essentially requested that:

- position deviation is lower than 0.2° in any condition without faults;
- post-fault position and speed are within the envelope defined in Figure 9.

Table 1: Relevant test cases (centred rigging).

ID	Torsion [Nm] Static	Torsion [Nm] 23.25 Hz	Bending [Nm]	Axial [N]	Radial [N]	Fault
A	209	29.5	29	725	1260	No
B.f4	235	0	0	0	0	Yes

3.2. Position-tracking and disturbance-rejection

The results obtained in terms of position tracking and load disturbance rejection during test A are presented in Figure 10. Initially (0 s < t < 14.6 s, Figure 10), the actuator is commanded to hold the centred position while the static value of the torsional is increased up to 209 Nm, and then the complete load scenario is imposed (14.6 s < t < 23.5 s, Figure 10). Successively (t > 23.5 s), the actuator is commanded to reach at constant speed (0.7°/s) its full-strokes (+/-5°), by stopping at centred and extreme positions. It can be noted that the position deviation, Figure 10(c), is well lower than the maximum allowable value (0.2°) in all working positions. Figure 10(c) also points out that the EMA stiffness depends on the working position, by roughly following a linear relationship.

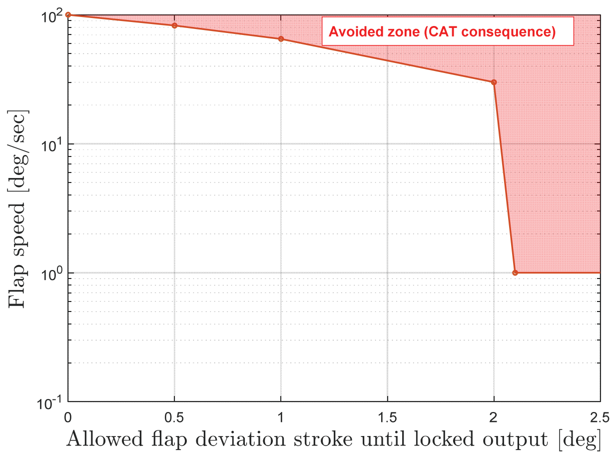

Figure 9: Post-fault envelope of output speed and position (requirement).

This behaviour is related to the variation of the torsional free length of the roto-translating screw of the mechanical transmission (Figure 5), which achieves minimum and maximum values when the position reaches -5° and 5°, respectively. In addition, the position deviation is characterized by peaks when the demand rate abruptly varies (t = 23.5 s; 32.1 s; etc.), so that its maximum is approximately 0.13° (t = 61 s).

3.3. Robustness against failures

The robustness against failures has been characterized by artificially injecting a major fault (section 2.6) while the EMA is moving at constant speed towards an endstroke and the maximum static torsional load (235 Nm) is applied in the direction of motion. The results reported in Figure 11 are related to test B.f4, in which a frozen value of the output angle feedback, potentially caused by a sensor malfunction or by a communication fault, is injected (t = 0 s, Figure 11(a)). After the fault injection, as a result of the linearly increasing error between the command and the frozen feedback signals, the actual speed increases roughly linearly (Figure 11(b)), and the output shaft position deviates from setpoint with roughly constant acceleration, Figure 11(a). When both fault symptoms related to the OSM exceed the thresholds the fault counter is triggered and, after the latency confirmation cycles, the fault is detected (t = 0.170 s, Figure 11). After the fault detection, the back-electromotive damper circuitry is activated, causing an immediate deceleration of the output shaft (the speed comes back under the threshold within 60 ms), and the brake is commanded to engage. The fault is considered completely compensated when the output speed reaches zero for the first time (t = 0.317 s, Figure 11), with a maximum position deviation of 0.48°.

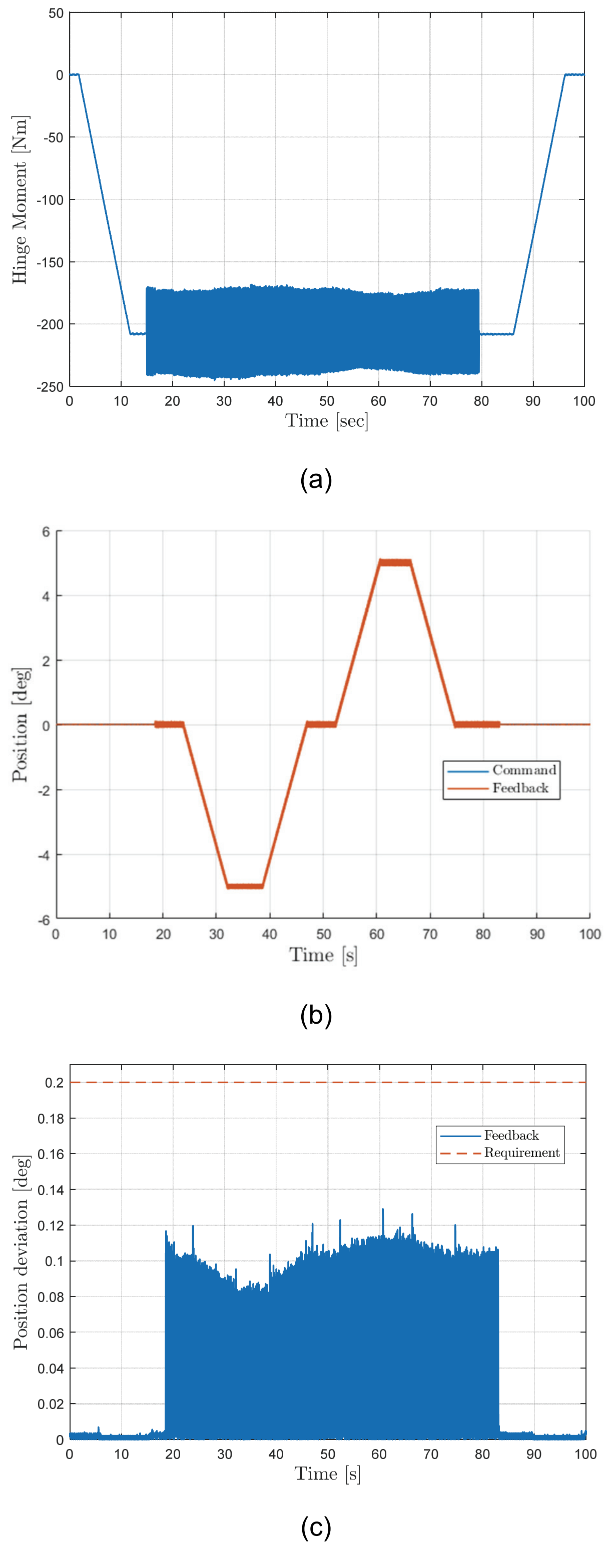

Figure 10: Experimental results during test A: torsional load (a); position feedback (b); position deviation (c).

Finally, Figure 12 represents the failure transient using the allowable post-fault envelope of speed and position deviation, demonstrating that the EMA is fully compliant with requirements.

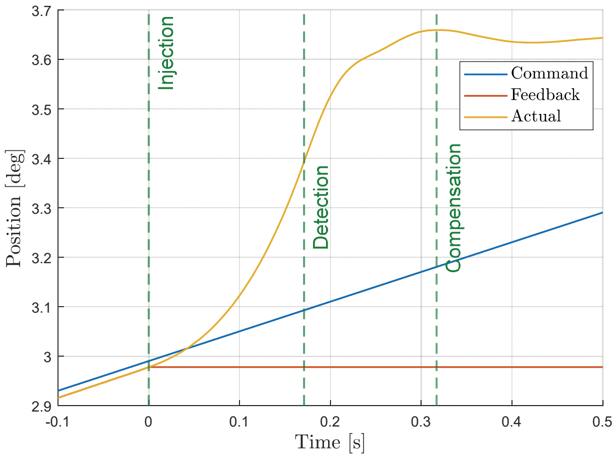

(a)

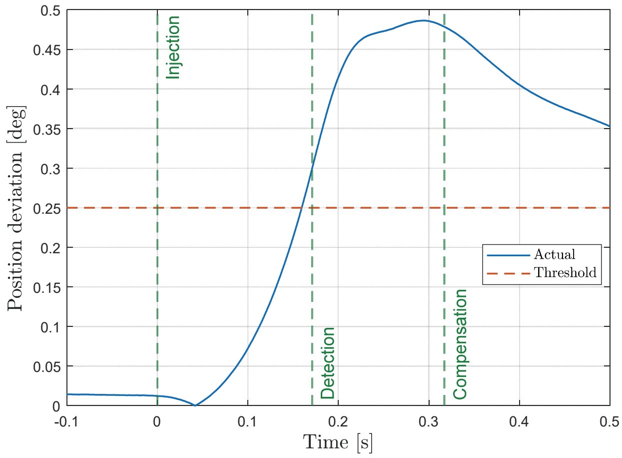

(b)

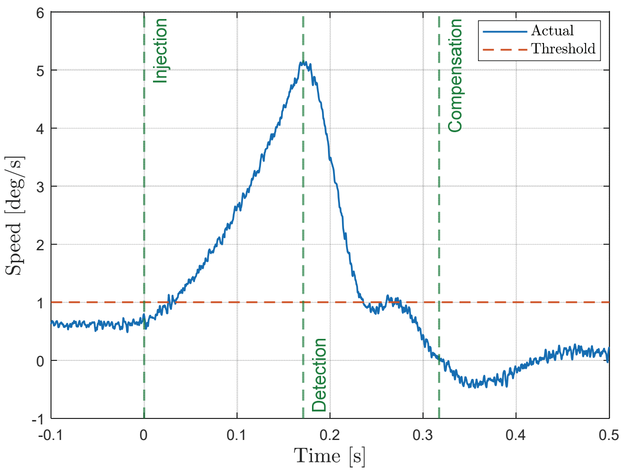

(c)

Figure 11: Failure transient characterisation during test B.f4: post-fault position (a); position deviation (b); actuator speed (c).

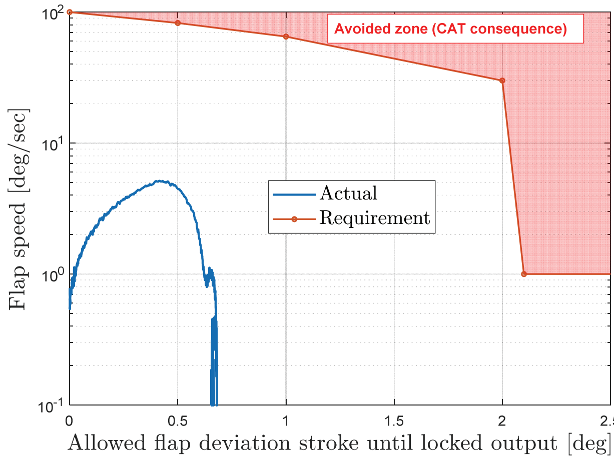

Figure 12: Post-fault envelope of position and speed (response).

4. CONCLUSIONS

The work summarizes the experimental activities carried out for the qualification of the EMA employed for the flap movables of the Airbus RACER helicopter-plane. The EMA performances in terms of position tracking and load disturbance-rejection are characterized under worst-case load scenarios, reproduced by a multi-axes hydraulic test rig applying torsional moment up to 209 Nm static, plus +/- 29.5 Nm at 23.25 Hz, as well as bending moment, axial and radial forces. During qualification, the position deviation in all working deflections is lower than 0.13°. Robustness against failures is also discussed, documenting the EMA response when a major fault is artificially injected (as worst case, the fault occurs while the EMA is moving at constant speed and the maximum static torsional load is applied in the direction of motion). In the worst conditions, the fault is detected within 170 ms and the EMA is completely locked by the brake (fail-safe mode) within 317 ms, with a maximum position deviation of 0.48°. Qualification tests also confirm the effectiveness of the power electronics design, which integrates a specifically-designed back-electromotive damper circuitry for the minimization of the failure transients of the EMA.

Authors' contacts:

Gianpietro Di Rito, gianpietro.di.rito@unipi.it

Romain Kovel, romain.kovel@airbus.com

Benedetto Luciano, b.luciano@aesis-studio.it

Federico Salvi, FSalvi@umbragroup.com

Marco Nardeschi, MNardeschi@umbragroup.com

5. REFERENCES

1. "Flightpath 2050: Europe's vision for aviation". Available online (accessed 30 July 2024): https://op.europa.eu/en/publication-detail/-/publication/7d834950-1f5e-480f-ab70-ab96e4a0a0ad/language-en

2. Maré, J.-C.; Fu, J. "Review on signal-by-wire and power-by-wire actuation for more electric aircraft". Chinese Journal of Aeronautics, 2017, Vol. 30 (3), pp. 857–870, DOI: 10.1016/j.cja.2017.03.013.

3. Madonna, V.; Giangrande, P.; Galea, M. "Electrical power generation in aircraft: review, challenges, and opportunities". IEEE Transactions on Transportation Electrification, 2018, Vol. 4 (3), pp. 646–659, DOI: 10.1109/tte.2018.2834142.

4. Schäfer, A.W.; Barrett, S.R.H.; Doyme, K.; Dray, L.; Gnadt, A.R.; Self, R.; O'Sullivan, A.; Synodinos, A.; Torija, A.J. "Technological, economic and environmental prospects of all-electric aircraft". Nature Energy, 2019, Vol. 4, pp. 160–166, DOI: 10.1038/s41560-018-0294-x.

5. Qiao, G.; Liu, G.; Shi, Z.; Wang, Y.; Ma, S.; Lim, T.C. "A review of electromechanical actuators for more/all electric aircraft systems". Proceedings of the Institution of Mechanical Engineering, Part C - Journal of Mechanical Engineering Science, 2018, Vol. 232, pp. 4128–4151, DOI: 10.1177/0954406217749869.

6. Gao, Z.; Cecati, C.; Ding, S.X. "A survey of fault diagnosis and fault-tolerant techniques - Part I: Fault diagnosis with model-based and signal-based approaches". IEEE Transactions on Industrial Electronics, 2015, Vol. 62 (6), pp. 3757–3767, DOI: 10.1109/tie.2015.2417501.

7. Gao, Z.; Cecati, C.; Ding, S.X. "A survey of fault diagnosis and fault-tolerant techniques - Part II: Fault diagnosis with knowledge-based and hybrid/active approaches". IEEE Transactions on Industrial Electronics, 2015, Vol. 62 (6), pp. 3768–3774, doi:10.1109/tie.2015.2419013.

8. Mazzoleni, M.; Previdi, F.; Scandella, M.; Pispola, G. "Experimental development of a health monitoring method for electro-mechanical actuators of flight control primary surfaces in more electric aircrafts". IEEE Access, 2019, Vol. 7, 153618–153634, DOI: 10.1109/access.2019.2948781.

9. Di Rito, G.; Luciano, B.; Borgarelli, N.; Nardeschi, M. Model-based condition-monitoring and jamming-tolerant control of an electromechanical flight actuator with differential ball screws. Actuators 2021, 10, 230. DOI: 10.3390/act10090230

10. Di Rito, G.; Kovel, R.; Nardeschi, M.; Borgarelli, N.; Luciano, B. "Minimisation of failure transients in a fail-safe electro-mechanical actuator employed for the flap movables of a high-speed helicopter-plane". Aerospace, 2022, Vol. 9, art. n. 527. DOI: 10.3390/aerospace9090527

11. Huot, R.; Eglin, P. "Flight Mechanics of the RACER compound H/C", In Proceedings of the 76th Vertical Flight Society's Annual Forum & Technology Display, Virginia Beach, Virginia, USA, Oct. 6-8, 2020.

12. Thiemeier, J.; Öhrle, C.; Frey, F.; Keßler, M.; Krämer, E. "Aerodynamics and flight mechanics analysis of Airbus Helicopters compound helicopter RACER in hover under crosswind conditions", CEAS Aeronautical Journal, 2020, Vol. 11, pp. 49–66, DOI: 10.1007/s13272-019-00392-3.

13. Stokkermans, T.; Veldhuis, L.; Soemarwoto, B.; Fukari, R.; Eglin, P. "Breakdown of aerodynamic interactions for the lateral rotors on a compound helicopter", Aerospace Science and Technology 2020, Vol. 101, DOI: 10.1016/j.ast.2020.105845.

6. CLASSIFICATION & COPYRIGHT